



ELSEVIER

Nuclear Instruments and Methods in Physics Research A 452 (2000) 205–222

**NUCLEAR
INSTRUMENTS
& METHODS
IN PHYSICS
RESEARCH**
Section A

www.elsevier.nl/locate/nima

CHICO, a heavy ion detector for Gammasphere[☆]

M.W. Simon*, D. Cline, C.Y. Wu, R.W. Gray, R. Teng, C. Long¹*Nuclear Structure Research Laboratory, University of Rochester, 271 East River Road, Rochester, NY 14623, USA*

Received 19 January 2000; accepted 7 March 2000

Abstract

A 4π position-sensitive heavy-ion detector system, CHICO, has been developed primarily for use in conjunction with the 4π γ -ray facility, Gammasphere. The CHICO detector comprises an array of 20 Parallel Plate Avalanche Counters (PPACs) covering $12^\circ < \theta < 85^\circ$ and $95^\circ < \theta < 168^\circ$ and 280° in ϕ . The PPACs have segmented delay-line cathode boards, measuring the polar scattering angle θ to 1° , and segmented anodes, measuring the azimuthal angle ϕ with 9° resolution, while measuring the time-of-flight difference with 500 ps resolution. For binary reactions the kinematics can be reconstructed from the measured information, allowing identification of the target- and projectile-like nuclei with a mass resolution of $\Delta m/m \approx 5\%$. The measured masses, recoil velocities, and recoil angles allow correction for Doppler shift and assignment of individual γ -rays to decay of the correct reaction product. This paper describes the design, operation and performance of the CHICO detector. The powerful combination of CHICO plus Gammasphere provides new research opportunities for the study of nuclear structure and reactions. © 2000 Elsevier Science B.V. All rights reserved.

PACS: 25.70 – z; 29.40.Cs; 29.40.Gx

Keywords: 4π charged particle detector; Position sensitive PPACs

1. Introduction

Recent development of 4π arrays of large, high-resolution, Ge γ -ray detectors, such as Gammasphere [1], has led to dramatic gains in both the γ -ray detection efficiency and the resolving power. This significant technical development has opened exciting new research opportunities leading to the

discovery and study of a variety of new physics (see, for example, Refs. [2,3]).

The selectivity of 4π arrays of high-resolution γ -ray detectors can be enhanced considerably by using them in conjunction with associated auxiliary detectors. This paper focuses on coincident detection of scattered heavy-ion reaction products, recoiling out of thin targets, in coincidence with the de-excitation γ -rays from the reaction products. This heavy-ion γ -ray coincidence technique provides the ability to select the reaction channel, determine scattering angles, select impact parameters, correct for the Doppler shift on an event-by-event basis, and identify which product emitted individual γ -rays.

[☆]All work supported by the National Science Foundation.

*Corresponding author. Tel.: 1-716-275-4316; fax: 1-716-473-5384.

E-mail address: simon@nsrl.rochester.edu (M.W. Simon).

¹Presently at Space Telescope Science Institute, Baltimore MD, USA.

For heavy-ion reactions the recoil velocities of the reaction products can be as high as $v/c = 10\%$, leading to appreciable Doppler shift of the γ -rays emitted from the nuclei in flight. As a consequence, γ -ray spectra from thick target experiments can suffer from appreciable Doppler-broadened line shapes for transitions that have lifetimes comparable to the stopping time of the recoiling nuclei in the target. By contrast, when thin targets are used, the excited nuclei recoil into vacuum and the Doppler-broadened line shapes can be significantly reduced if the recoil directions and velocities are determined. Measurement of the time-of-flight difference, plus the scattering angles of the recoiling nuclei, allows reconstruction of the kinematics of the reaction, and distinguishes the target-like from the projectile-like nuclei for two body reactions. Measurement of the scattering angles and velocities of the reaction products allows the γ -ray energies to be corrected for the Doppler effect on an event-by-event basis, resulting in spectra with high γ -ray energy resolution and the ability to assign the γ -rays to the target- or projectile-like nucleus from the observed Doppler shift.

The heavy-ion γ -ray coincidence technique is especially powerful for study of quasi-binary reactions such as Coulomb excitation, nucleon transfer, and fission. Large solid angle heavy-ion detectors make it possible to concurrently measure scattering angles and γ -ray yields over a range of scattering angles. For Coulomb excitation experiments this is equivalent to measuring γ -ray yields for varying Coulomb excitation strength, giving information on the $B(E\lambda)$ values of the excited levels [4–6]. The scattering angle information also can be used to preferentially select reactions that occur near the grazing angle, selectively enhancing the transfer channels [7]. The coincident γ -rays can be used to identify the correlated reaction products determining the number of nucleons transferred. Large solid angle heavy-ion detectors also can be used to study three-body reactions such as charged-particle-induced fission, etc.

The paper described development of a large solid-angle particle detector, CHICO (Compact Heavy Ion Counter) that was designed specifically to exploit the particle- γ -ray coincidence technique with Gammasphere, although it has more general

applications. The CHICO heavy-ion detector is based on experience using two generations of box-shaped PPAC detectors arrays followed by the “Ice cream Cone” detector array, all developed at Rochester [8,9]. During the past two decades these previous detector arrays were used extensively for studies of heavy-ion-induced Coulomb excitation and transfer reactions. The combination of CHICO plus Gammasphere provides a tremendous advance in detector capability compared to prior detector arrays opening exciting new research opportunities.

2. The CHICO detector

2.1. Design requirements

There are several factors constraining the design of a heavy-ion detector to be used successfully in conjunction with Gammasphere. The heavy-ion detector design and performance must address the experimental requirements for the physics being studied. Furthermore the heavy-ion detector must be designed to have a minimal impact on the performance of Gammasphere, while the geometry and 37.5 cm inner diameter of the central cavity of Gammasphere places stringent constraints on the physical size and symmetry of the heavy-ion detector.

The primary purpose of the heavy-ion detector is to gather enough information from the involved nuclei to reconstruct the kinematics of the event. For binary reactions the measurement of the scattering angles of both target- and projectile-like nuclei define the momenta of the recoiling nuclei through the relation derived from conservation of momentum, with the assumption of two-body kinematics

$$P_{1,2} = \frac{P_0 \sin(\theta_{2,1})}{\sin(\theta_1 + \theta_2)} \quad (1)$$

where P_0 is the momentum of the incident beam, P_1 and P_2 are the momenta of the recoiling nuclei, and θ_1 and θ_2 are the scattering angles. Resolution of the measured polar scattering angles to 1° is sufficiently accurate to calculate the momenta of

the nuclei since other effects, such as the size of the beam spot, produce comparable errors in the angle measurement. Measurement of the azimuthal angle ϕ for each detector is needed to ensure that both scattered nuclei are coplanar as required for binary reactions.

The scattering angles of the nuclei completely define the momenta for two-body reactions but, in practice, do not uniquely identify the target- and projectile-like nuclei over the full range of scattering angles. The CHICO detector uses the difference in time-of-flight of the two recoiling nuclei to resolve the two scattering solutions. For the geometry of the CHICO detector, the minimum flight path from the target to the detectors is about 13 cm, and, for experiments run near the Coulomb barrier, the separation in time-of-flight difference for the two solutions is typically on the order of nanoseconds. Therefore, in order to resolve the two solutions over all scattering angles, it is critical to use detectors with sub-nanosecond time resolution.

Parallel plate avalanche counters (PPACs) [10] are ideally suited for heavy-ion detection in the proposed application. They can be designed with sufficient angular resolution and typically have time resolutions around 300 ps (FWHM). In addition, PPACs have other attractive features for this application. The individual detectors can handle particle detection rates around 100 k/s, leaving experimental detection rates limited only by the acquisition electronics. The PPACs are resistant to radiation damage, can run for months with good stability, and the detection threshold for heavy ions can be adjusted to the experiment. This latter feature is especially valuable for cases such as ^{252}Cf fission studies where the α -decay rate is about 31 times the fission rate, making it important to tune the PPACs to be insensitive to the α -particles. The PPACs can be designed to have light-mass and be constructed of low Z materials so they weakly scatter γ -rays, and hence minimize degradation of the performance of Gammasphere.

The symmetry chosen for the particle detector is dependent on the symmetry of Gammasphere. For certain experimentally measurable quantities, such as the excitation of the nuclei as a function of the scattering angle (or equivalently the impact parameter), or γ -ray angular distributions, it is use-

ful to sum spectra that originate from sets of γ -ray detectors having the same angular positions with respect to particle scattering angles, in order to minimize the total number of spectra to be analyzed. The particle detector should have the same symmetry as the Ge detectors of Gammasphere in order to maximize the number of spectra that can be summed. The γ -ray detectors of Gammasphere are arranged with pentagonal symmetry, but the particle detector needs to have an even number of detectors to effectively collect binary particle coincidences, therefore, CHICO was designed with the least common multiple of 10 azimuthal sections.

2.2. CHICO description

The CHICO detector consists of 20 separate trapezoidal parallel plate avalanche counters (PPACs). There are two identical hemispherical assemblies, each of which houses 10 of the PPACs arranged in a truncated cone coaxial with the beam direction (Figs. 1 and 2). Fig. 3 shows one hemisphere of the CHICO detector installed in one half of Gammasphere. The PPACs, their segmented anodes, and their delay line cathodes are described in Section 2.3. The two hemispherical assemblies are joined along the $\theta = 90^\circ$ plane (with respect to the beam direction). The forward assembly has an

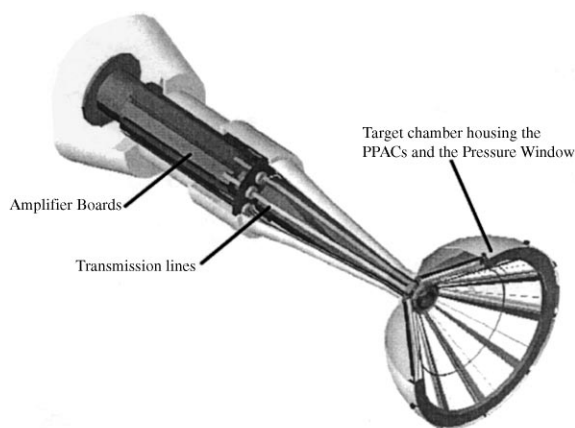


Fig. 1. Sectional view of CHICO. The target chamber housing the PPACs and the pressure window is on the right. The transmission lines carrying the signals from the PPACs to the amplifier boards also can be seen. The length of the assembly is 91 cm.

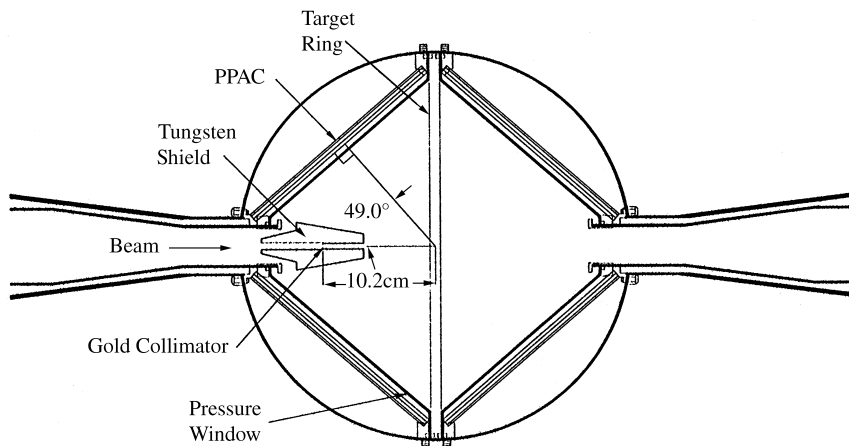


Fig. 2. Cross-sectional view of the CHICO target chamber. The heavy lines show the vacuum envelope containing the gas volume.

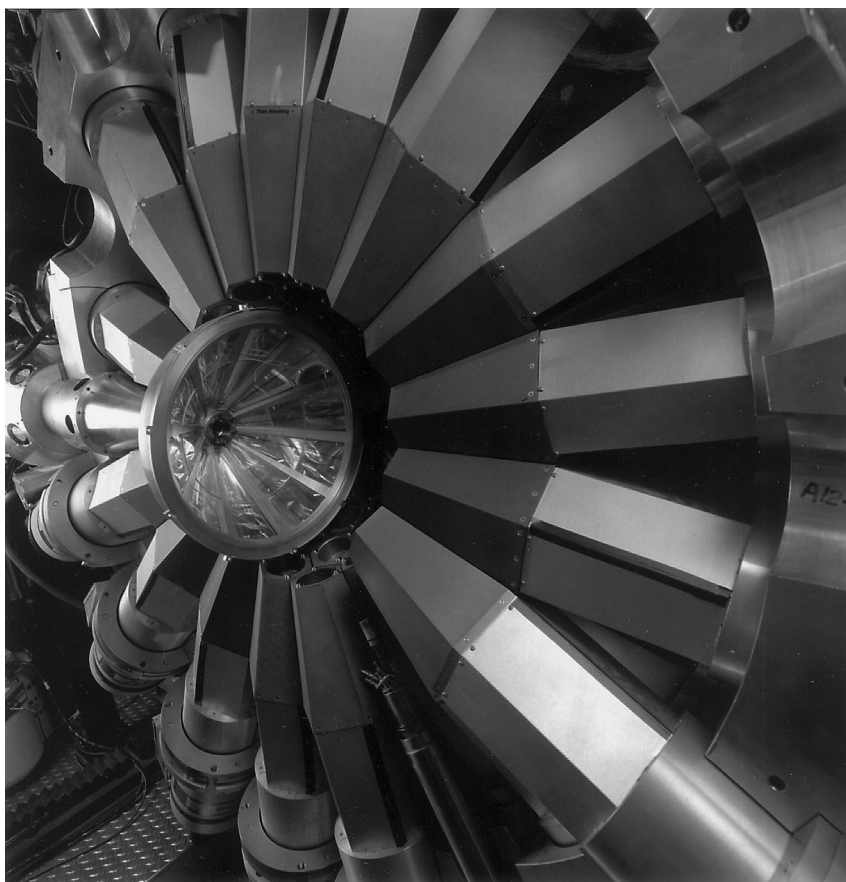


Fig. 3. One half of CHICO coupled with one half of Gammasphere.

active θ range from 12 to 85° , and the back assembly has an active θ range from 95 to 168° . An individual PPAC covers an azimuthal width of 28° , and there is a dead region of 8° in ϕ between each of the PPACs, giving 280° of ϕ coverage for both the forward and back assemblies. The total angular coverage is $\sim 2.8\pi$ sr, or about 69% of the total solid angle. About 20% of the total solid-angle is lost to the dead space between the PPACs, another 9% is lost along the joint between the two halves, and 2% is lost at the beam entrance and exit ports. Note that the joint between the two halves also coincides with the plane of the target and thus also is unusable due to heavy-ion scattering in the target. The PPACs are positioned with the normal at an angle of 49° with respect to the beam axis and the minimum flight path, from the center of the target to the midpoint between the anode and cathode in the PPACs, is 12.8 cm.

The housing for the PPACs is a 1.58 mm (0.0625 in) thick aluminum hemisphere shell with a 35.6 cm (14 in) diameter. The PPACs are mounted to fixtures epoxied to the inside of the hemisphere. The epoxy used was Hysol EA 9309.3NA, manufactured by Dexter Aerospace Materials Division, and was chosen for its high shear and peel strength with aluminum. The wide end of the PPACs are seated in a ring glued along the diameter of the hemisphere, which also provides the O-ring seal with the pressure window. The pressure window consists of

a conical frame covered with 0.9 μm thick Mylar ($120 \mu\text{g}/\text{cm}^2$), and serves to contain the detector gas from the target chamber high vacuum volume (Fig. 4). All 10 PPACs for each hemisphere of CHICO sit in a common gas volume. A collimator can be mounted in the target chamber. This tungsten collimator has a 6.4 mm (0.25 in) diameter entrance hole and a 5.1 mm (0.2 in) exit hole and holds a gold foil with a 3.2 mm (0.125 in) diameter hole 10.2 cm (4 in) from the target. The collimator has no more than 12% transmission for a 600 keV γ -ray which may arise from excitation of the gold foil by the beam.

The target ladder can hold four targets at one time and is designed so that the targets can be switched without opening the detector (Fig. 4). The ladder is mounted on a 9.5 mm (0.375 in) thick ring that has the same diameter as the hemisphere, with an O-ring on each side. This annular ring of the target ladder assembly completes the vacuum seal between the two hemispheres of the CHICO detector. Two separate target ladder assemblies have been constructed, one of which allows the targets to be retracted into a closed box to facilitate handling of radio-active targets. Both target ladders are insulated so a bias voltage up to 5 kV can be applied to suppress the emission of secondary electrons. Suppression of secondary electron emission is crucial for reliable detector operation when using very heavy-ion beams.

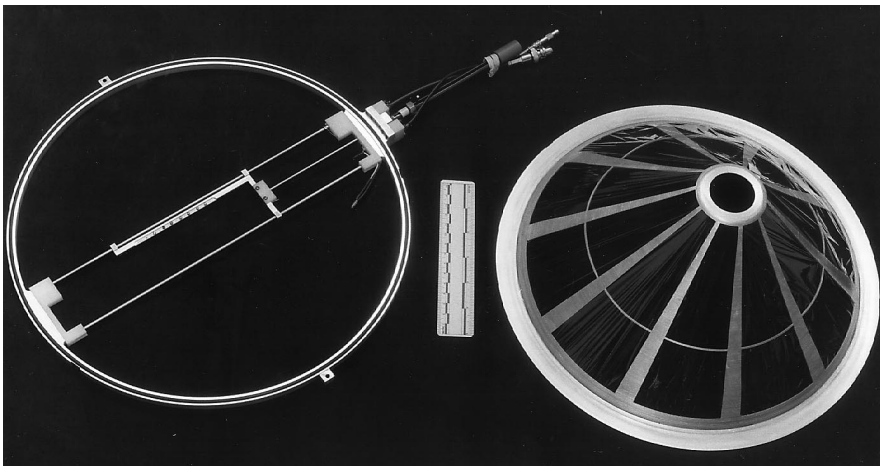


Fig. 4. Photograph of the target holder ring plus ladder and a pressure window.

The upstream hemisphere of CHICO, which contains the beam collimator, is supported rigidly by the upstream beam line. The downstream CHICO hemisphere is supported by a compact assembly housing a high vacuum pump, a Faraday cup, and telescope system for viewing the target. This compact downstream assembly is mounted on a kinematic mount that allows the two hemispheres to be separated along the beam axis in order to remove and insert the target ring.

2.3. PPACs

The essential elements of each PPAC comprise a thin film anode plus a cathode circuit board. A diagram of an individual PPAC assembly is shown in Fig. 5. The anode, made of approximately $100 \mu\text{g}/\text{cm}^2$ thick stretched polypropylene with an approximately $20 \mu\text{g}/\text{cm}^2$ aluminum coating, is glued to a 3.2 mm (0.125 in) thick G10 frame. The aluminum coating is segmented into two electrically isolated sections to provide azimuthal angle segmentation, one segment is 9.3° wide and the other 18.6° wide. The aluminum segments on the stretched polypropylene were made by vacuum deposition with the back of the anode foil cooled by 0.5 Torr of helium. The vacuum deposition was performed by clamping the rear of the anode frame against an O-ring on a similar shaped chamber that is mounted inside the vacuum evaporator. Helium was passed through this chamber during the vac-

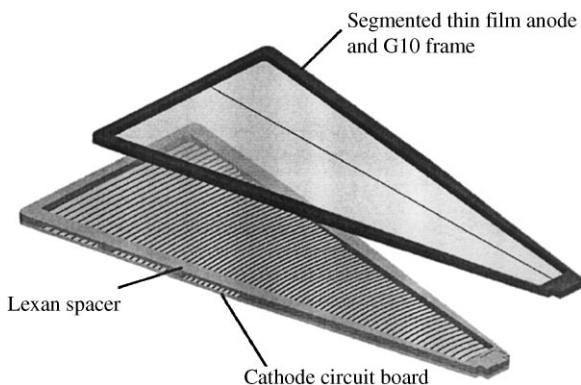


Fig. 5. Assembly of an individual PPAC. The asymmetrically segmented anode and the cathode board with the attached Lexan spacer are shown.

uum deposition. The helium cooling was essential to produce coatings with good electrical properties, anode foil coatings made not using helium cooling were found to have dead areas.

A 3.2 mm (0.125 in) thick Lexan spacer separates the anode from the cathode. The spacer is slotted along the sides so the detector gas can circulate to the active region of the PPAC, preventing degradation of the detector performance over time due to radiation damage of the gas. The azimuthal width of the spacer is 28 and 30° for the anode frame. The spacer has a smaller opening angle to prevent edge effects, where the aluminized polypropylene is glued to the anode frame, from causing an electrical discharge to the cathode. The azimuthal width of the active area of the PPACs (defined by the spacer) is constant, so the total geometric ϕ acceptance remains constant at 78% over the entire polar range of the full detector assembly.

The cathode board is a three layer circuit board, shown in Fig. 6. The active side (front) of the cathode board, where the particles are detected, is segmented into 1° wide traces of constant polar angle θ . Each of the traces is connected to one tap of a delay line which is mounted on the back side of the cathode board. The delay line has a delay of 1 ns per tap and is made of passive delay chips

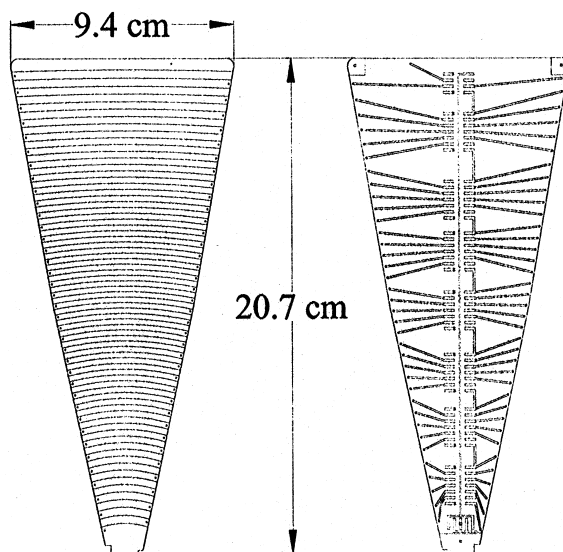


Fig. 6. Front and back of a cathode board.

manufactured by Rhombus Industries. The traces on the active side of the board are connected to the delay line on the back of the cathode board by plated-thru holes which are located near the edge of the board. The third (middle) layer is a ground plane located between the delay line side and the active side of the cathode. The ground plane acts to capacitively decouple the traces of the delay line on one side of the board from the sensing traces on the active side of the board. The addition of the ground plane considerably improves the performance of the delay line.

The signals from the anode and cathode are carried to the amplifiers by a stripline transmission line that has four $50\ \Omega$ impedance traces on a central plane shielded on either side by ground planes. The PPAC end of the transmission line is forked, allowing two of the traces to connect to the cathode board and two of the traces to the segmented anode. The anode traces on the transmission line also carry the bias voltage ($\sim 400\ \text{V}$) to the PPAC anode. Fig. 7 shows a photograph of an anode, a cathode board, transmission line and amplifier board.

2.4. Electronics

2.4.1. Amplifiers

Compact amplifier boards were designed at the Nuclear Structure Research Laboratory specifically for use with the CHICO detector. Each PPAC has a dedicated amplifier board with two anode channels and two cathode channels. The physical size of the boards was kept small, $26.7\ \text{cm} \times 3.2\ \text{cm}$, allowing them to be housed in the detector assembly as close to the PPAC detectors as possible to reduce electronic noise pickup. The amplifiers are based on cascadable microwave amplifier chips, simplifying the design and construction. A schematic diagram of the amplifier circuits is shown in Fig. 8. The amplifier circuit boards are three-layer boards, with the signal traces on the middle layer shielded by ground planes. Since the acquisition electronics require negative inputs with pulse heights on the order of a Volt, the anode amplification chain is non-inverting with a total gain of 400, while the cathode amplification chain is inverting with a gain of 700. The 500 MHz bandwidth of the amplifiers ensures that the rise times of the pulses

are not degraded during amplification. A photograph of one amplifier board is shown in Fig. 7. The geometrical arrangement of transmission lines and amplifier boards is illustrated in Fig. 1.

2.4.2. Acquisition electronics

A schematic figure of the acquisition electronics is shown in Fig. 9. Standard NIM and CAMAC modules are used to extract and digitize the time information from the amplified anode and cathode signals. The time pick-off signals from both the anodes and cathodes are converted to logic pulses by Tennelec model 454 Constant Fraction Discriminators (CFDs). The logic timing signals then travel through 130 ns of delay cables and are regenerated and converted to ECL standard logic pulses by LeCroy model 3412 discriminators. The LeCroy 3412 discriminators have two outputs, one which passes the signal on to the time-to-digital converters (TDCs), and the other which can be used in conjunction with scalar units to monitor signal rates during an experiment. The TDCs are a combination of the LeCroy model 4303 Fast Encoding and Readout TQCs (FERETs) and the LeCroy model 4300B Fast Encoding Readout ADCs (FERAs). The charge output from each FERET is further delayed by 265 ns and fed into a FERA unit, where the signals are digitized and stored until read into the data stream. The FERET units are run in a common stop mode and are gated at the first level trigger rate. The charge outputs are started in the individual channels of the FERETs upon receipt of the timing signal from the LeCroy model 3412 discriminators and are stopped at the end of the gate signal.

The gates for the FERETs are provided by a LeCroy model 4508 Programmable Lookup Unit (PLU). This unit provides a flexible method of generating a valid event (or gate) signal and can be programmed to accommodate various experimental conditions. The anode signals of the full PPAC array are summed by quadrant (front right, front left, back right, back left) after the CFDs, and these summed signals are the inputs to the PLU. The PLU generates the first level trigger if the conditions for a valid particle event are satisfied. The final trigger requires a coincidence of a valid charged particle event with a selected multiplicity

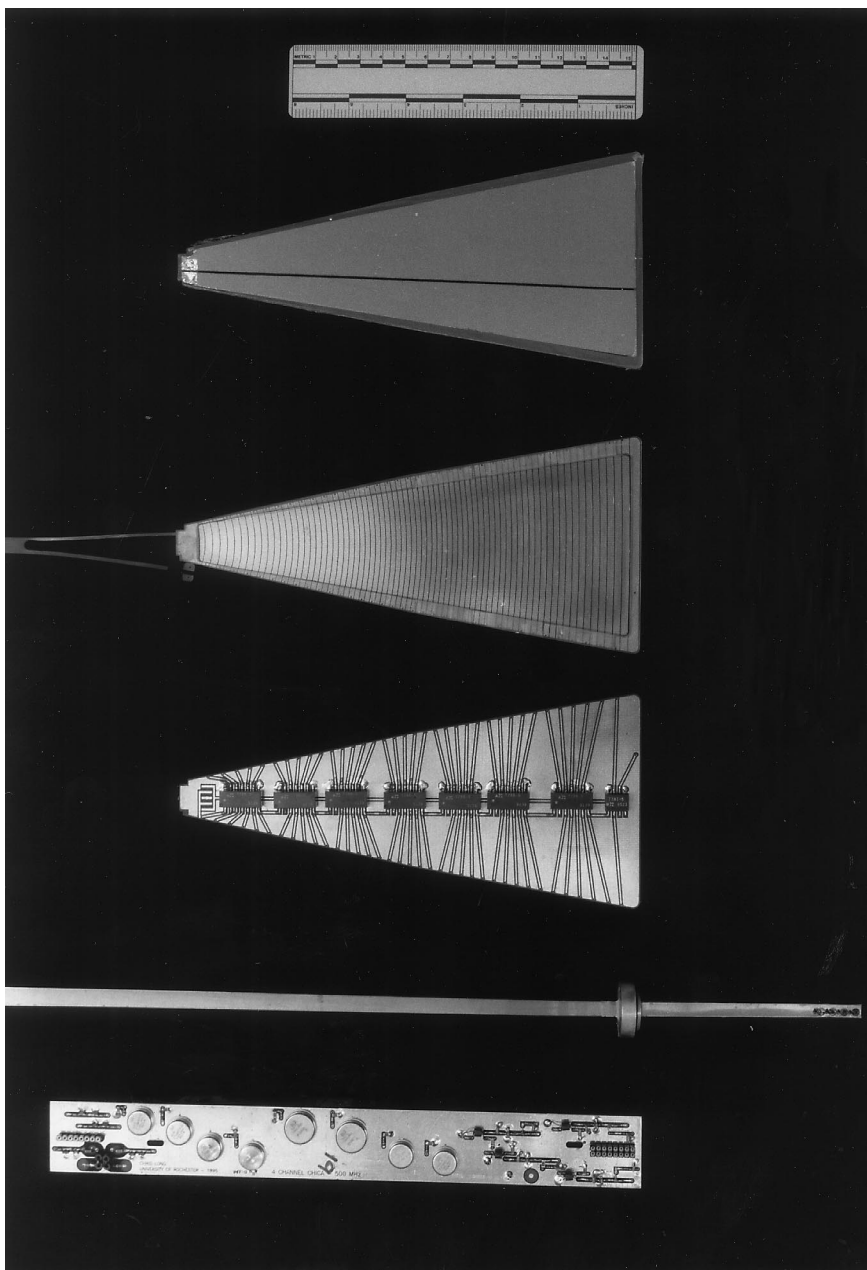


Fig. 7. Photograph (from top down) of individual anode foil, active side of a cathode board with attached transmission line, delay-line side (back) of cathode board, a separate transmission line, and one amplifier board.

of γ -rays. This final trigger is used to gate the FERAs and to inform the Gammasphere data acquisition system that the event should be read and entered into the data stream.

2.5. Gas control system

The detector gas used in the PPACS is instrument grade isobutane at a pressure of 4 Torr. There

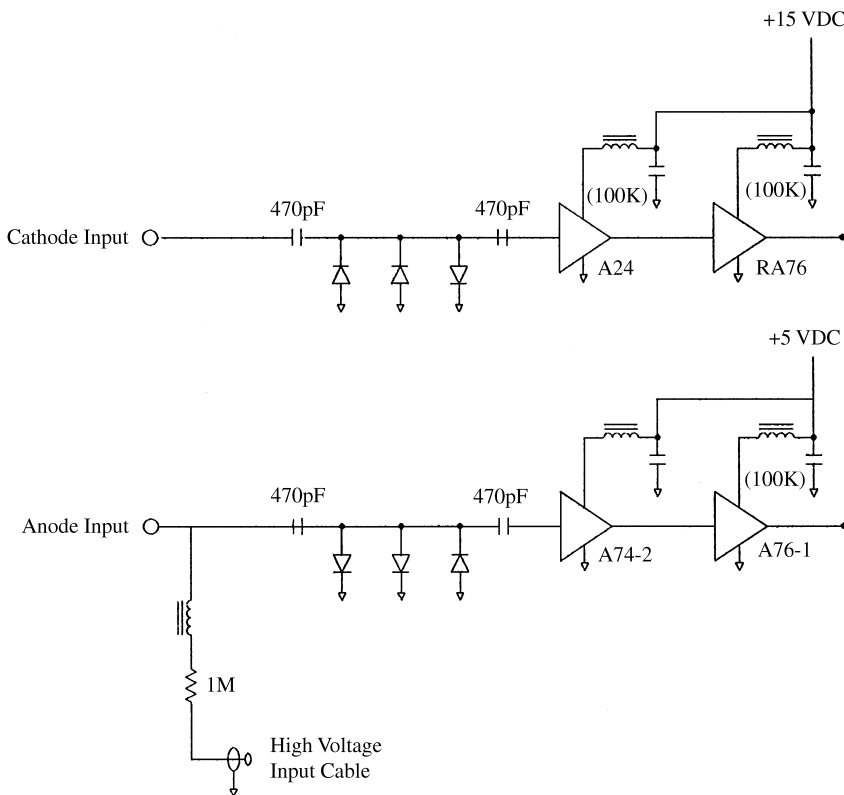


Fig. 8. Circuit diagram for the anode and cathode amplifiers. The amplifier chips were manufactured by Watkins-Johnson.

are two gas volumes, one for each hemisphere of the detector, and 10 PPACs are housed within each volume. The circulation and pressure of the isobutane for each volume is controlled by an independent gas handling system. A schematic of the gas handling systems is shown in Fig. 10. The pressure difference across of the pressure window is monitored by a 10 Torr MKS 233B differential Baratron gauge, and this pressure difference is maintained by a MKS 250 controller and associated valve. The absolute pressure is monitored by a 1000 Torr Baratron gauge while the flow rate is monitored by a MKS 1259 mass flow meter.

3. Detector performance

3.1. Position measurement and calibration

The detector was designed to measure both the polar (θ) and azimuthal (ϕ) angles (with respect to

the beam direction) of the scattered nuclei. The ϕ measurement is provided by the segmentation of the anodes. A “binary” scheme was implemented, similar to previous generations of Rochester heavy-ion detectors [8,9], to reduce the number of electronic channels necessary for the given ϕ resolution. The anodes are segmented into two sections covering $\frac{1}{3}$ and $\frac{2}{3}$ of the ϕ -angle subtended by the individual PPACs. Two-body kinematics demand that the scattered beam-like and recoiling target-like nuclei are co-planar, so the combination of large and small segments, in which the reaction products are detected, define the ϕ -slice in which the reaction plane lies (Fig. 11). The ϕ -resolution is $\sim \pm 4.7^\circ$ and is limited by the angular width of the smaller of the two anode segments, which is 9.3° . The ϕ -measurement is defined by the geometry of the detector and the combination of the anodes in which the nuclei are detected.

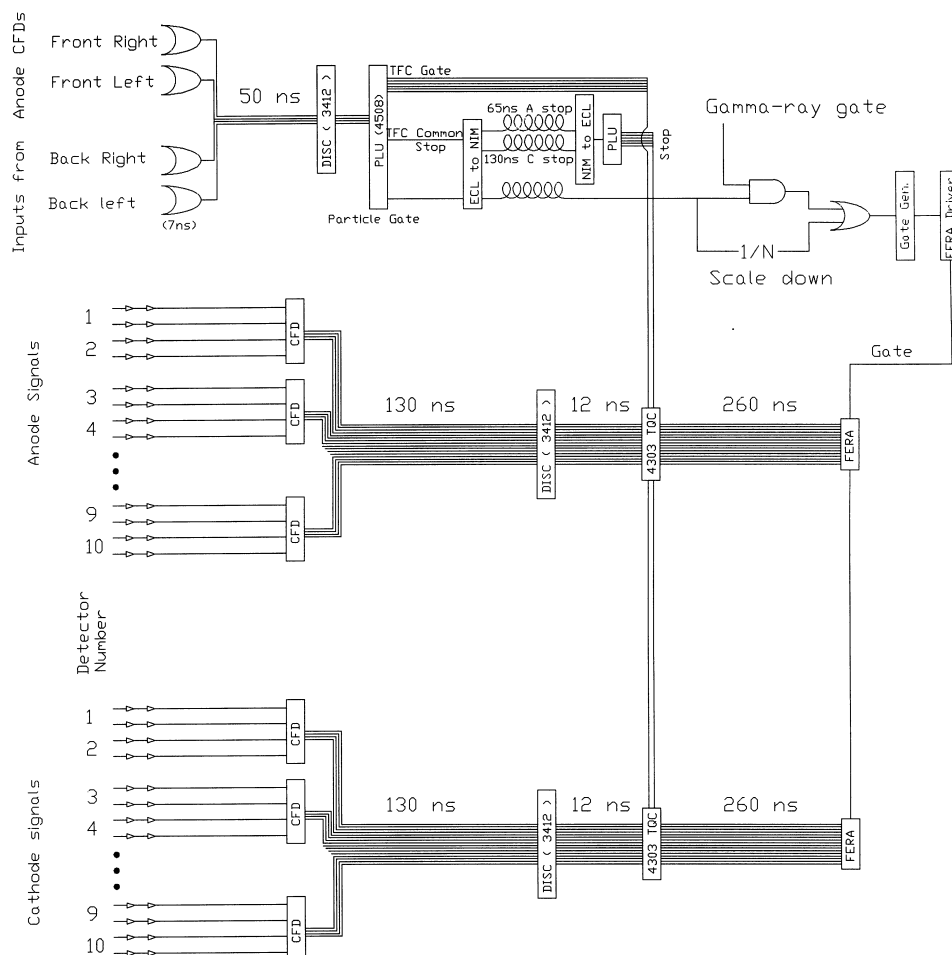


Fig. 9. Schematic of the acquisition and trigger electronics. Only one half of the anode and cathode electronics is shown.

The θ -angle measurement is obtained from the signals read out of the delay line on the cathode board. The signal generated in the cathode by the incident heavy ion travels both directions down the delay line. The time difference between the two ends of the delay line determines the location of the event along the delay line. An example of the position measurement is shown in Fig. 12. This spectrum contains events in which the target and projectile nuclei were detected in coincidence in the reaction ^{86}Kr on ^{63}Cu at a lab energy of 265 MeV. The peaks in the spectra correspond to the 1° spacing of the θ slices on the cathode board, indicating that the position resolution is about 1° . The

dip in the position spectrum near 60° is the shadow of a support rib in the pressure window, which subtends 1° . The dip in the spectrum at 25° results from the coincidence particle-detection requirement since this is the scattering angle for Kr corresponding to when the Cu is blocked by the support rib in the opposite PPAC. Also present in the position spectrum is the maximum scattering angle of 47° for the Kr nuclei. The sharp cutoff at 20° is from a mask to eliminate small scattering-angle events. The cutoff beyond 67° is also a result of the coincidence requirement, reflecting that the Kr is masked below 20° .

The position measurement for an individual PPAC can be calibrated using the geometrical

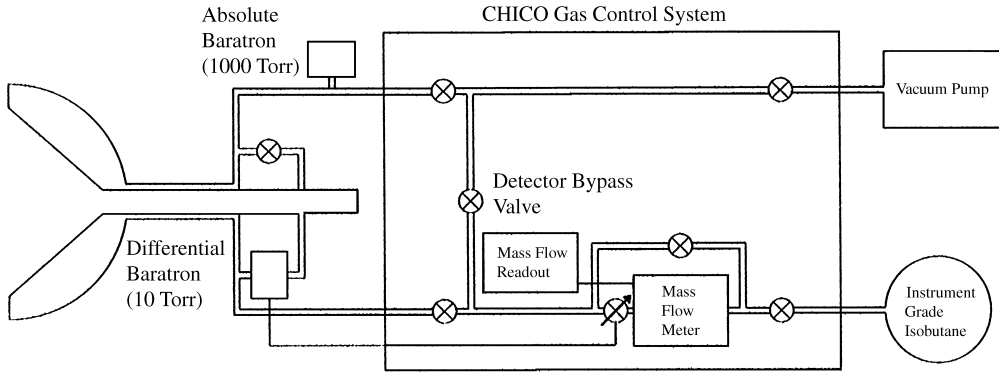


Fig. 10. The CHICO gas control system.

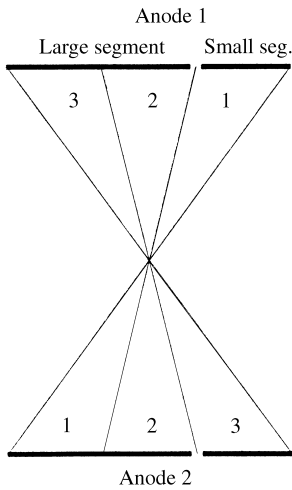


Fig. 11. Segmentation of anode pairs. Co-planar anode pairs (front–front and front–back) are segmented in a way to uniquely define the ϕ of the reaction plane. For example, if the large section of both anodes trigger, then the reaction plane is in ϕ slice 2.

limits and the shadow of the support rib as reference points. A more precise calibration can be performed by relying on the angular correlation of scattered ions following elastic scattering. The position measured in one PPAC is plotted against the position measured in the opposing PPAC, and these curves are then fit to the calculated kinematic angular correlations. There are two kinematic curves in these plots corresponding to either the projectile- or target-like nucleus arriving in one of the PPACs. There is one unique angle where these

Position Spectrum

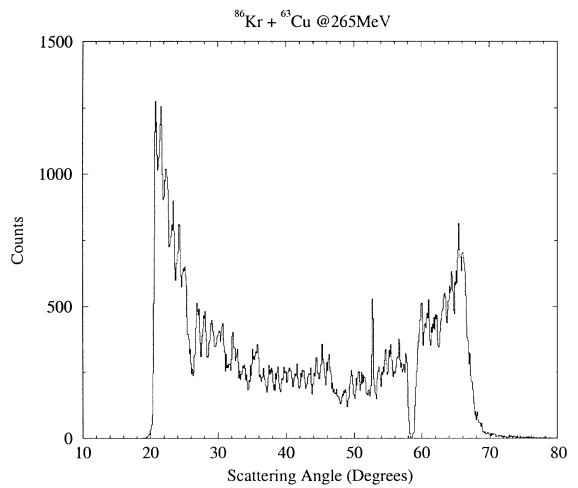


Fig. 12. Scattering-angle position spectrum. The various features of the position spectrum are discussed in the text of Section 3.1.

kinematic curves cross, defined in the lab frame by

$$\theta_{\text{cross}} = \cos^{-1}\left(\frac{1}{2}\sqrt{1 + \frac{m_{\text{proj}}}{m_{\text{targ}}}}\right) \quad (2)$$

where m_{proj} and m_{targ} are the mass of the projectile and target, respectively. Matching this point in the data, to the calculated value, defines a family of possible calibration coefficients. Since the angular correlations can be relatively featureless (as can be seen for the $^{144}\text{Sm} + ^{248}\text{Cm}$ reaction in Fig. 13), it

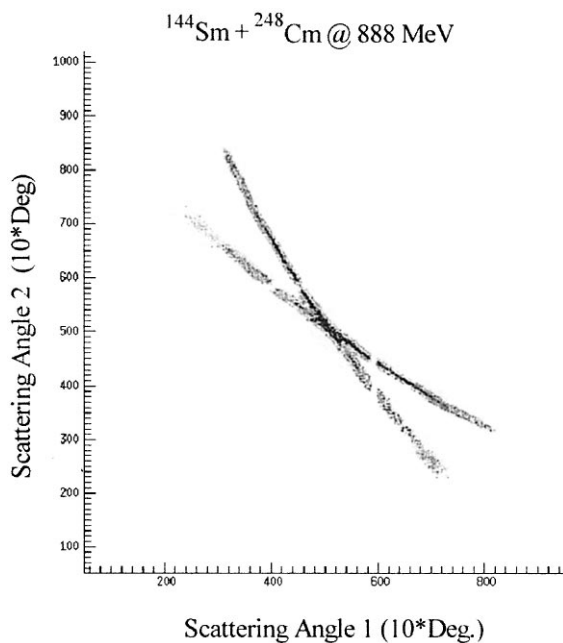


Fig. 13. The angular correlations of the scattered nuclei into two opposing PPACs are used to calibrate the position measurement. The gap at 60° caused by the shadow of the support rib in the pressure window.

may not be possible to pick the calibration coefficients unambiguously. Adding a second data set with m_{proj} and m_{targ} chosen so that θ_{cross} is significantly different provides a method of choosing the correct values for the calibration.

The back array of PPACs ($\theta > 90^\circ$) were calibrated in a similar manner, except instead of using beam on target data, a thin source fission was used. The fission fragments leave the source co-linearly, so the sum of the polar angles of their flight direction must add to 180° . The calibrations for the back PPAC positions can then be determined by reference to the front PPAC positions. Again, a least-squares fit was performed for each of the 10 front-back pairs of PPACs, but with the coefficients for the front PPACs fixed by the beam-on-target calibration.

3.2. Time measurement and particle identification

For binary reactions the target- and projectile-like nuclei can be identified if they are detected in

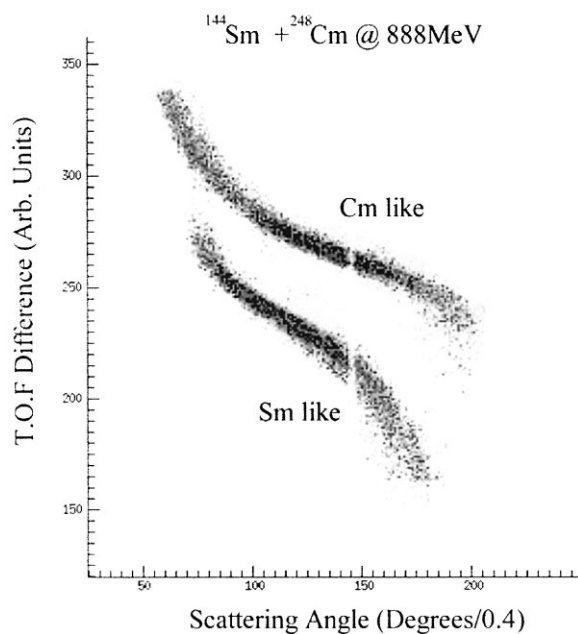


Fig. 14. Particle identification. Measurement of the time-of-flight difference and scattering angles allows the two scattering solutions to be cleanly separated. The time difference for the two solutions is 6.6 ns at 45° (i.e. channel 112).

coincidence by plotting the scattering angle versus the time-of-flight difference (Δ_{TOF}). An example of this is shown in Fig. 14.

The resolution of the time-of-flight difference measurement is about 0.7 ns. The various experimental factors contributing to the time resolution for a typical beam experiment, in this case a beam of 780 MeV (lab energy) ^{162}Dy on a $250 \mu\text{g}/\text{cm}^2$ ^{118}Sn target, can be calculated and are shown in Table 1. Typical values for the energy (E_{strag}) and angle (θ_{strag}) straggle of the beam and ejectile nuclei as they pass through the target material are shown, along with their contribution to the time resolution. The location of the reaction within the target material also effects the time of flight, since the beam and scattered nuclei lose energy as they pass through the target material. This contribution to the time resolution is listed in Table 1 under “Target Thickness”. The largest contribution to the time resolution uncertainty is the beam spot size. Because of the short flight path (~ 13 cm) to the detectors, the 3 mm beam spot subtends about 1°

Table 1

Contributions to the time resolution for 780 MeV ^{162}Dy on a $250 \mu\text{g}/\text{cm}^2$ ^{118}Sn target

Time resolution (ns)	
Measured width	~ 0.7
E_{strag}	
Dy (0.8 MeV)	~ 0.01
Sn (0.6 MeV)	~ 0.04
θ_{strag}	
Dy (0.3°)	~ 0.05
Sn (0.1°)	~ 0.02
Target thickness	~ 0.1
Beam spot (3 mm)	~ 0.4
Electronic resolution	~ 0.2
Intrinsic resolution	~ 0.52

with respect to a given point on the detectors. The energy of the scattered nuclei varies rapidly enough with scattering angle for this to be the major contribution to the time resolution. The resolution of the electronics was measured to be 0.2 ns. The intrinsic time-difference resolution, after unfolding all of these contributions, is about 500 ps, or 350 ps for a single PPAC.

The mass of each nucleus can also be calculated with the assumption of two-body kinematics by

$$m_1 = \frac{\Delta_{\text{TOF}_{1,2}} + (d_2/P_2)M_{\text{tot}}}{(d_1/P_1) + (d_2/P_2)} \quad (3)$$

where $\Delta_{\text{TOF}_{1,2}}$ is the time-of-flight difference for the left and right nucleus, and d_1 and d_2 are the length of the flight path for the left and right nuclei, respectively. The momenta of the left and right nuclei ($P_{1,2}$) are given by Eq. (1). A calculated mass spectrum is shown in Fig. 15 for the reaction $^{144}\text{Sm} + ^{248}\text{Cm}$ at a lab energy of 888 MeV. The angular and time resolution of the detector allow a mass resolution of about 5% for in-beam experiments, sufficient to resolve the nuclei even for cases where the target and projectile masses are similar, such as $^{238}\text{U} + ^{208}\text{Pb}$ (Fig. 15).

3.3. γ -Rays

For heavy-ion reactions the nuclei can have large recoil velocities and, hence, the de-excitation γ -rays

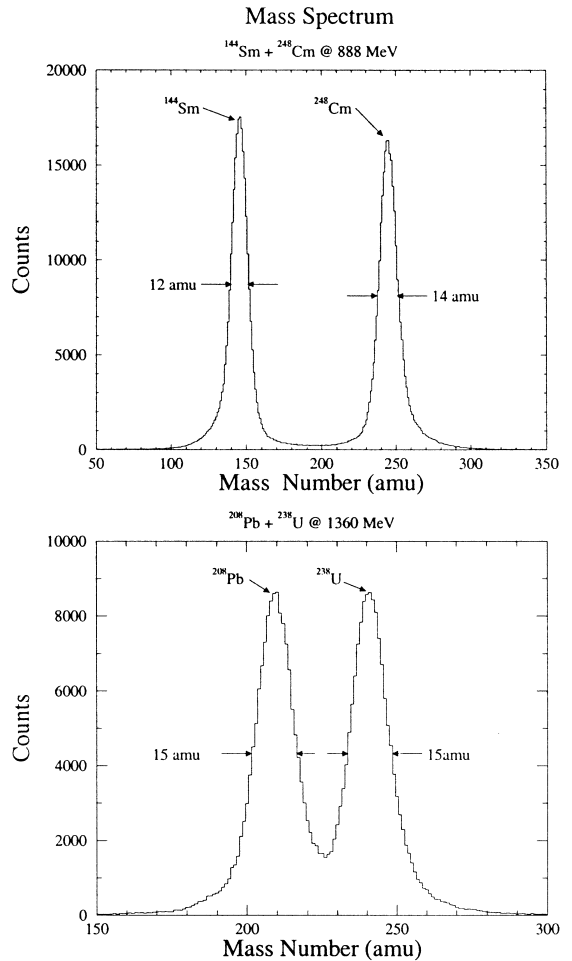


Fig. 15. Measured mass spectrum from the reaction $^{144}\text{Sm} + ^{248}\text{Cm}$ at 888 MeV (upper) and $^{208}\text{Pb} + ^{238}\text{U}$ at 1360 MeV (lower).

can have large Doppler shifts. With the measurement of the reaction kinematics and identification of the target- and projectile-like nuclei, the appropriate Doppler correction can be applied on an event by event basis. The Doppler correction provides a powerful way to identify which reaction product emitted a particular γ -ray. This is simulated in Fig. 16 for fission of ^{252}Cf , where the light fission fragment is assumed to emit a 500 keV γ -ray that is detected by Gammasphere. Sharp line shapes are obtained only when the emitted γ -ray is attributed to the correct fragment. An example of

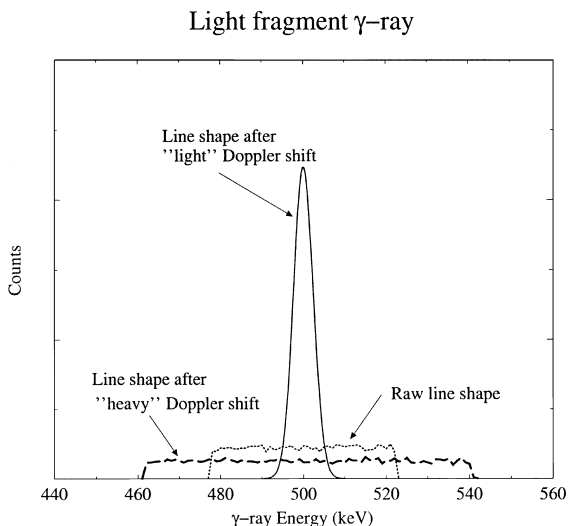


Fig. 16. Simulation of the γ -ray line shapes obtained for a 500 keV γ -ray transition emitted by the light fragment following spontaneous fission of a ^{252}Cf source. This figure shows the raw line shape and the line shapes obtained by correcting for the Doppler effect assuming emission from either the light or heavy fission fragment.

this is given by the γ -ray spectra from the reaction $^{238}\text{U} + ^{170}\text{Er}$ at $E_{\text{lab}} = 1358$ MeV [12] which is shown in Fig. 17. The γ -ray line shapes in the raw (uncorrected) spectra (Fig. 17a) are Doppler broadened and difficult to identify. The application of the Doppler correction appropriate for the target-like nucleus (Fig. 17b) or projectile-like nucleus (Fig. 17c) on the same data set recovers the sharp γ -ray line shapes and provides a method of associating the γ -rays unambiguously with the target- or projectile-like nuclei.

The Doppler correction assumes a point γ -ray detector, and consequently the γ -ray energy resolution achieved is limited by the variation of the Doppler shift over the finite aperture of any γ -ray detector. That is, the γ -ray energy resolution (dE/E), after making the Doppler correction, is given by

$$\frac{dE}{E} \approx \beta \sin(\theta_{\text{py}}) \Delta\theta \quad (4)$$

where β is the recoil velocity, θ_{py} is the opening angle between the direction of the γ -ray and recoil

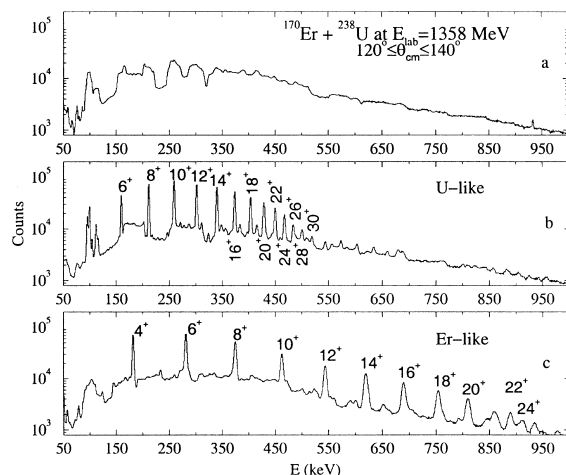


Fig. 17. Typical γ -ray spectra. (a) shows the raw γ -ray spectra for the reaction $^{170}\text{Er} + ^{238}\text{U}$ at $E_{\text{lab}} = 1358$ MeV; (b) and (c) show the spectra after Doppler correction using the kinematics measured with the CHICO detector. The spin labels are for transitions in ^{238}U (b) and ^{170}Er (c).

direction of the nucleus, and $\Delta\theta$ is effectively the opening angle of the γ -ray detectors. The experimentally achieved γ -ray energy resolution, summed over all Gammasphere detectors, typically is around 1.0% because it is dominated by this finite detector size effect. The poorer energy resolution of the ^{170}Er γ -rays in Fig. 17c compared to the ^{238}U γ -rays in Fig. 17b is a result of the larger recoil velocities of the ^{170}Er nuclei. Many of the Gammasphere detectors have two-fold segmentation which allows better location of the γ -ray interaction region in the Ge detectors. This segmentation can be used to slightly improve the achieved energy resolution. For example, a 1 MeV γ -ray emitted by ^{170}Er , for the above reaction, gives an energy resolution for the total Doppler-corrected γ -ray spectrum of 1.3% using the centroid angle of individual Ge detectors, which improves to 1.1% when the segmentation is exploited.

3.4. Performance of Gammasphere with CHICO

The impact of CHICO on the response characteristics of Gammasphere is an important consideration when coupling these two detectors. The CHICO detector was designed with low Z material,

GEANT Simulation of Peak Efficiency

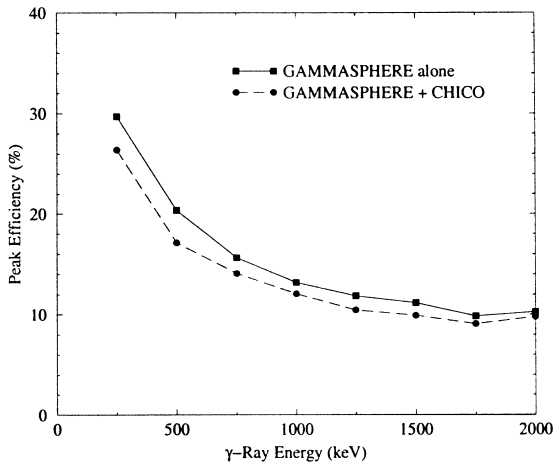


Fig. 18. GEANT simulation of the effect of CHICO on the peak efficiency of Gammasphere for γ -rays emitted at the target location.

GEANT Peak to Total Simulation

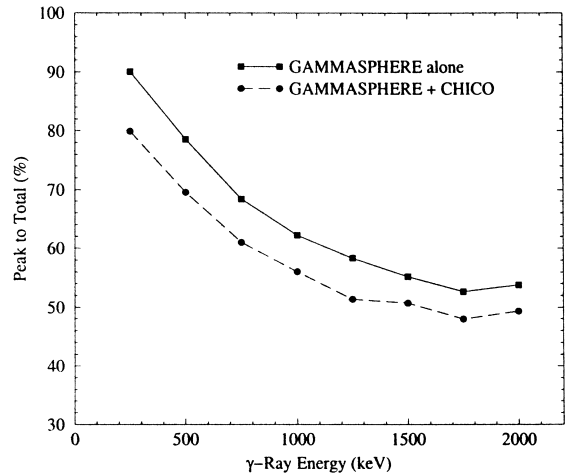


Fig. 19. GEANT simulation of the effect of CHICO on the peak-to-total ratio of Gammasphere for γ -rays emitted at the target location.

and as little mass as possible within the scattering chamber of Gammasphere, to minimize scattering and absorption of γ -rays. Simulations modeling the influence of CHICO on the response of Gammasphere were performed using the Monte Carlo code GEANT [11]. The peak efficiency (Fig. 18) and the peak-to-total ratio (Fig. 19) for Gammasphere were modeled with and without the presence of CHICO. The peak efficiency simulation over predicts the performance of Gammasphere, giving a value of 11.8% compared to the measured value of 9.9%. The simulation shows that the presence of CHICO decreases the calculated peak efficiency of Gammasphere from 11.8% to 10.4% for a 1.25 MeV γ -ray. The simulations reproduce the measured peak-to-total ratio of 0.6 quite accurately for a 1.25 MeV γ -ray and indicate that the influence of CHICO reduces the peak-to-total ratio from 58.3% to 51.3%.

3.5. Operating experience

Operation of CHICO detector array has proven it to be reliable, stable and easy to use even at high count rates. The PPAC detectors and pressure window show no signs of degradation after several

weeks of in-beam experiments even using very heavy ion beams such as ^{238}U . The only problem encountered has been in achieving sufficient shielding of the high-gain high-bandwidth amplifiers in order to block oscillation and cross talk. Careful shielding of the amplifiers, plus removal of the energy output channels from the PPAC amplifiers has eliminated these problems. The impact of the several days required to set up CHICO with Gammasphere has been minimized by scheduling the running of several experiments in series.

4. Physics applications

Heavy-ion reactions used in conjunction with high-resolution γ -ray spectroscopy, is the pre-eminent technique for studying nuclear structure at high spin and isospin. The recent development of high detection efficiency 4π arrays of large Ge γ -ray detectors, such as Gammasphere, makes it possible to study high-fold γ -ray coincident events, leading to dramatic improvements in selectivity and sensitivity. This technical development opened exciting new research opportunities leading to discovery and study of a variety of new physics [2,3].

CHICO adds the ability to perform kinematic reconstruction for heavy-ion reactions, determine scattering angle, mass, Q -value, correct for Doppler shift and make unambiguous assignment of γ -rays to individual reaction products. The synergy provided by combining CHICO and Gammasphere further advances research opportunities for the study of nuclear structure. The most obvious applications are to studies of binary reactions, such as heavy-ion Coulomb excitation or transfer reactions, as well as quasi-binary reactions such as fission. As illustrated in Fig. 17 CHICO plus Gammasphere finally makes it possible to study γ -ray spectroscopy even when both interacting nuclei are strongly deformed or have odd mass. This technical capability has important applications. The following three examples are given to illustrate the capabilities of CHICO plus Gammasphere for study of nuclear structure physics.

4.1. Coulomb excitation

Heavy-ion Coulomb excitation is the pre-eminent probe of collective shape degrees of freedom in nuclear structure. The scattering angle provided by CHICO is crucial for quantitative Coulomb excitation work, and the high-fold γ -ray information from Gammasphere provides an enormous advance in selectivity and sensitivity for studies of multiple collective bands in nuclei [4–6]. Coulomb excitation data recorded for a wide range of projectile Z values and scattering angles is sufficient to determine uniquely the complete set of $E\lambda$ matrix elements involving the low-lying states excited; see Refs. [4–6]. These directly determine the intrinsic frame $E\lambda$ moments which are the significant collective shape degrees of freedom. The sensitivity of CHICO plus Gammasphere for Coulomb excitation work is illustrated by the fact that it enabled study of the ground band states in ^{238}U up to spin 34 [12,13] while multiple side bands exhibiting unusual band interactions were observed to high spin in ^{162}Dy and ^{170}Er [12,14]. Another application was the first measurement of the octupole double-phonon 6^+ strength in ^{208}Pb and ^{96}Zr . This strength was found to be heavily fragmented in ^{208}Pb [13,15] whereas about 50% of the octupole double-phonon strength was observed at

$2h\omega$ in ^{96}Zr [6,16]. CHICO plus Gammasphere is an especially sensitive probe of isomeric states; this has been exploited to study the mechanism leading to strong population via Coulomb excitation of high- K isomeric states in ^{170}Er and ^{178}Hf [12,17].

4.2. Heavy-ion induced transfer reactions

The study of light-ion-induced few nucleon transfer reactions has contributed significantly to our understanding of nuclear structure in many aspects. Single-nucleon transfer is a direct probe of single-particle shell structure while two-nucleon transfer is a direct probe of pairing correlations in nuclei. CHICO plus Gammasphere dramatically expands the possibilities of exploiting heavy-ion-induced few nucleon transfer reactions to probe single-particle and pairing correlations to much higher spin in a wider range of nuclei. Moreover, the ability to resolve the levels, independent of whether the interacting nuclei are deformed, or odd mass, greatly expands the arsenal of available nuclei that can be used, allowing selection of the optimum Q -value for a particular transfer channel. The study of heavy-ion-induced few nucleon transfer reactions offers unique opportunities to investigate many intriguing aspects of physics [7]. For example, it can be used to selectively populate high- j orbits in actinide nuclei, or inelastic excitation accompanied by pair-transfer allows one to study the spin dependence of pairing correlations in two-nucleon transfer reactions. Diaboloic pairing transfer [18–20], which is a manifestation of Berry phase [21] in nuclei, is a special case of pair transfer across a band crossing. Enhancement for multi-nucleon transfer [22] between two colliding superfluid nuclei, at subbarrier energies, could lead to the nuclear Josephson effect [23]. Recently CHICO plus Gammasphere were used to study pair correlations in nuclei, in particular, the quenching of pairing with increasing spin, as well as a search [14] for nuclear analogs of the Josephson effect in quasi-elastic scattering of ^{162}Dy by ^{118}Sn . It was found that the $4n$ transfer is not as enhanced as predicted [22]. Another example was the use of transfer reactions to discover new states, up to spins $45/2^+$, 22^+ and $61/2^+$ in neutron-rich nuclei

^{171}Er , ^{172}Er and ^{237}U [12], respectively, while yrast states in the neutron-rich nucleus ^{166}Dy were observed to spin 16^+ [24]. Isomers in ^{171}Er and ^{237}U were observed in a recently completed experiment [12].

4.3. Fission-fragment spectroscopy

Weakly bounded neutrons in neutron-rich nuclei may have interesting implications for nuclear structure, such as possible modifications of shell structure and new modes of excitation. Very little is known about the nuclear spectroscopy of neutron-rich nuclei due to the paucity of reactions populating such nuclei. Fragmentation in fission, either spontaneous or induced by charged particles, is an ideal method for populating levels to high spin in neutron-rich nuclei. The advent of large Ge arrays, such as Eurogam or Gammasphere, generated renewed interest in the spectroscopic study of neutron-rich fission products [25,26]. Early experiments used sealed sources, that is, the detected γ -rays were emitted while the fission products were stopping inside the source, producing Doppler-broadened line shapes for transitions from higher-spin states. The interwoven γ -rays from both correlated fission partners and from the 700 fission channels make unique assignments for weak transitions or weak channels impossible. Additional selectivity, other than the high-fold of γ -rays detected by the Eurogam or Gammasphere arrays, is required to expand fission fragment spectroscopy. A unique selectivity is introduced by using a thin-backed open source to allow coincident detection of both fission fragments in coincidence the deexcitation γ -rays. From the reconstructed fission kinematics, one can measure the masses of fission fragments and velocity vectors for Doppler-shift corrections of detected γ -rays. The mass selectivity increases the sensitivity for weak channel selection in fission while the Doppler-shift corrections allow identification of the fission fragment from which the γ -rays originated. In addition this method produces sharp lines for fast transitions that would have Doppler-broadened line shapes due to γ -ray emission during stopping in a thick source. This thin-target technique was developed using the Gammasphere array coupled to CHICO with

a $\simeq 70 \mu\text{Ci } ^{252}\text{Cf}$ on a $\simeq 500 \mu\text{g}/\text{cm}^2$ nickel foil [27,28]. This system provided 8 mass unit resolution, and a sensitivity to products produced with a yield of 5×10^{-5} /fission was achieved by mass gating. This work extended rotational bands up to $20\hbar$ for many highly neutron-rich nuclei providing information on the evolution of nuclear structure with spin. For example, rotational bands studied to high spin in $^{112,113,114,115,116}\text{Pd}$, and $^{111,113}\text{Rh}$ showed that the band crossings are due to $(\nu h\frac{1}{2})^2$ aligned configurations consistent with prolate deformation [28]. A second back-bend was observed at ^{116}Pd , while the γ -band in ^{112}Ru exhibits evidence for triaxial deformation to high spin. This technique has been extended to study neutron-rich $50 < A < 90$ nuclei via fusion–fission in the reaction of ^{48}Ca with ^{130}Te [29]. There is considerable interest in this mass region both from the point of view of nuclear spectroscopy and for the role of populated nuclei in the astrophysical r-process. Note that CHICO plus Gammasphere is ideally suited to study both the fission process and neutron-rich nuclei populated by transfer or strongly damped reactions.

5. Summary

CHICO, a 4π position-sensitive, heavy-ion detector system, has been developed primarily for use in conjunction with the 4π γ -ray facility, Gammasphere. The CHICO detector comprises an array of 20 Parallel Plate Avalanche Counters (PPACs) covering $12^\circ < \theta < 85^\circ$ and $95^\circ < \theta < 168^\circ$ and 280° in ϕ giving an angular coverage of 2.8π sr. The PPACs have segmented delay-line cathode boards, measuring scattering angle θ to 1° , segmented anodes, measuring azimuthal angle ϕ with 9° resolution, while the time-of-flight difference is measured with 500 ps resolution. For binary reactions the kinematics can be reconstructed from the measured information, allowing identification of the target- and projectile-like nuclei with a mass resolution of $\Delta m/m \approx 5\%$. The measured mass, recoil velocities and recoil angles allow correction for Doppler shift and assignment of individual γ -rays to decay of the correct reaction product. The detector has a minimum amount of mass within the Gammasphere

scattering chamber, and hence minimally degrades the response characteristics of Gammasphere. The design of the detector included development of compact high-gain amplifiers and a strip line transmission line, allowing the amplifiers to be placed within the detector housing, reducing problems with electronic noise.

The CHICO detector has become an important part of the Gammasphere program. Three examples are given to illustrate the power of this instrument to exploit heavy ions in order to study a variety of physics via Coulomb excitation, heavy-ion-induced transfer reactions and neutron-rich fission fragment spectroscopy.

References

- [1] M.A. Deleplanque, R.M. Diamond (Eds.), *Gammasphere, A National Gamma-ray Facility, The Proposal*, March 1988, Lawrence Berkeley Lab. Publ., 1988, p. 5202.
- [2] I.Y. Lee, in: M.A. Deleplanque, I.Y. Lee, A.O. Macchiavelli (Eds.), *Proceedings of the Workshop on Gammasphere Physics*, World Scientific, Singapore, 1995, p. 50.
- [3] M.A. Riley (Ed.), *GAMMASPHERE The Beginning ... 1993–1997*.
- [4] D. Cline, *An. Rev. Nucl. Part. Sci.* 36 (1986) 683.
- [5] L. Hasselgren, D. Cline, in: F. Iachello (Ed.), *Proceedings of the International Conference on Interacting Bose-Fermi Systems in Nuclei*, Plenum Press, New York, 1981, p. 241.
- [6] D. Cline, *Acta Physica Polonica B* 30 (1999) 1291.
- [7] C.Y. Wu, W. von Oertzen, D. Cline, M.W. Guidry, *An. Rev. Nucl. Part. Sci.* 40 (1990) 285.
- [8] D. Cline, B. Kotlinski, *UR-NSRL Biennial Report 1982–83*, p. 363.
- [9] D. Cline, E.G. Vogt, J. Hall, A.E. Kavka, W.J. Kernan, *UR-NSRL Annual Report 1987*, p. 149.
- [10] H. Stelzer, *Nucl. Instr. and Methods A* 133 (1976) 409.
- [11] R. Brun, F. Bruyant, M. Maire, A.C. McPherson, P. Zancarini, *GEANT, version 3.159, GEANT3 User's Guide, DD/EE/84-1*, CERN, 1987.
- [12] C.Y. Wu, D. Cline, M.W. Simon, R. Teng, K. Vetter, M.P. Carpenter, R.V.F. Janssens, I. Wiedenhover, *Phys. Rev. C* 61 (2000) 021305 (R).
- [13] K. Vetter, A.O. Macchiavelli, S.J. Asztalos, R.M. Clark, M.A. Deleplanque, R.M. Diamond, P. Fallon, I.Y. Lee, F.S. Stephens, D. Ward, H. Amro, R.V.F. Janssens, J. Gerl, H.-J. Wollersheim, D. Cline, M.W. Simon, C.Y. Wu, 1999, Unpublished.
- [14] C.Y. Wu, M.W. Simon, D. Cline, G.A. Davis, A.O. Macchiavelli, K. Vetter, 1998, Unpublished.
- [15] K. Vetter et al., *Phys. Rev. C* 58 (1998) R2631.
- [16] D. Cline, G. Davis, C.Y. Wu, M.W. Simon, R. Teng, I.Y. Lee, A.O. Macchiavelli, K. Vetter, *Proceedings of Nucl. Phys. Fall Meeting; Bull. Amer. Phys. Soc.* 43 (1998) 1584; in preparation.
- [17] Ch. Schlegel, A.B. Hayes, D. Cline, J. Gerl, T. Härtlein, E. Lubkiewicz, M. Rejmund, M.W. Simon, K. Vetter, H.J. Wollersheim, C.Y. Wu, 1999, Unpublished.
- [18] R.S. Nikam, P. Ring, *Phys. Rev. Lett.* 58 (1987) 980.
- [19] L.F. Canto, P. Ring, Y. Sun et al., *Phys. Rev. C* 47 (1993) 2836.
- [20] K.G. Helmer, C.Y. Wu, D. Cline, A.E. Kavka, W.J. Kernan, E.G. Vogt, M.W. Guidry, X.L. Han, R.W. Kincaid, X.T. Liu, H. Schecter, J.O. Rasmussen, A. Schihab-Eldin, M.A. Stoyer, M.L. Halbert, *Phys. Rev. C* 48 (1993) 1879.
- [21] M.V. Berry, *Proc. Roy. Soc. London, Ser. A* 392 (1984) 45.
- [22] J.H. Sorensen, A. Winther, *Phys. Rev. C* 47 (1993) 1691.
- [23] K. Dietrich, *Ann. Phys. (New York)* 66 (1971) 480.
- [24] C.Y. Wu, M.W. Simon, D. Cline, G.A. Davis, A.O. Macchiavelli, K. Vetter, *Phys. Rev. C* 57 (1998) 3466.
- [25] I. Ahmad et al., *Rep. Prog. Phys.* 58 (1995) 1415.
- [26] J.H. Hamilton et al., *Prog. Part. Nucl. Phys.* 35 (1995) 635.
- [27] M.W. Simon et al., in: J.H. Hamilton, A.V. Ramayya (Eds.), *Proceedings of the International Conference on Fission and Properties of Neutron Rich Nuclei*, Sanibel Island, FL, World Scientific, Singapore, 1998, p. 270.
- [28] M.W. Simon, Ph.D. Thesis, University of Rochester, 1999 unpublished.
- [29] M. Devlin, R.J. Charity, F.L. Lerma, D.G. Sarantites, D. Cline, M.W. Simon, C.Y. Wu, 1999, Unpublished.